Controllable Growth Orientation of Ag2O and Cu2O Films by Electrocrystallization from Aqueous Solutions

ARTICLE *in* CRYSTAL GROWTH & DESIGN · NOVEMBER 2012

Impact Factor: 4.89 · DOI: 10.1021/cg300813z

CITATIONS
9

READS
36

8 AUTHORS, INCLUDING:

Tsutomu Shinagawa
Osaka Municipal Technical Research Institute
71 PUBLICATIONS **795** CITATIONS
SEE PROFILE

Mitsuru Watanabe
Osaka Municipal Technical Research Institute
52 PUBLICATIONS **476** CITATIONS
SEE PROFILE

Minoru Inaba
Doshisha University
209 PUBLICATIONS **6,142** CITATIONS
SEE PROFILE

Akimasa Tasaka
Doshisha University
131 PUBLICATIONS **2,210** CITATIONS
SEE PROFILE

CRYSTAL GROWTH & DESIGN

Article

pubs.acs.org/crystal

Controllable Growth Orientation of Ag_2O and Cu_2O Films by Electrocrystallization from Aqueous Solutions

Tsutomu Shinagawa,*[,†] Yuya Ida,[‡] Kotaro Mizuno,[‡] Seiji Watase,[†] Mitsuru Watanabe,[†] Minoru Inaba,[‡] Akimasa Tasaka,[‡] and Masanobu Izaki[§]

[†]Electronic Materials Research Division, Osaka Municipal Technical Research Institute, Joto-ku, Osaka 536-8553, Japan

[‡]Graduate School of Engineering, Doshisha University, Kyotanabe, Kyoto 610-0321, Japan

[§]Department of Mechanical Engineering, Toyohashi University of Technology, Toyohashi, Aichi 441-8580, Japan

Supporting Information

ABSTRACT: We demonstrate that Ag_2O and Cu_2O polycrystal films with a cubic cuprite structure can be grown on F:SnO_2 substrates with controllable crystal orientation between ⟨111⟩ and ⟨100⟩ directions by galvanostatic electrocrystallization from aqueous electrolytes. The Ag_2O and Cu_2O films have been electrodeposited at different applied current densities determined by linear-sweep voltammetry (LSV) measurements, and their crystal structure and morphology were characterized with X-ray diffraction (XRD) and field emission scanning electron microscopy (FESEM). The XRD results show the preferred growth orientation changed from ⟨111⟩ to ⟨100⟩ with increasing and decreasing current density for Ag_2O and Cu_2O, respectively. The surface morphology, especially for the Cu_2O films, was also changed from a three-sided pyramidal shape to a four-sided pyramidal shape corresponding to the orientation. We also give a reasonable explanation for the observed trend in the growth orientation by considering the formation rate of AgOH and CuOH; higher and lower rates appear to yield ⟨111⟩ and ⟨100⟩ preferred orientation, respectively.

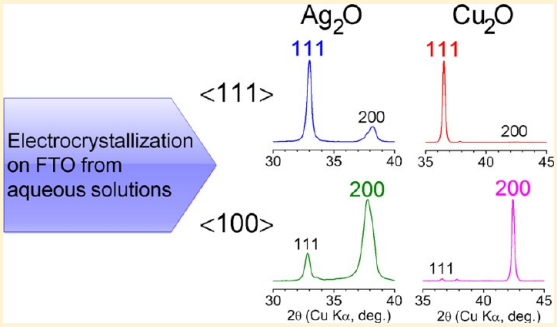

1. INTRODUCTION

Among binary oxides, silver(I) oxide (Ag_2O) and cuprous oxide (Cu_2O) are intrinsic p-type semiconducting materials, having the same cubic cuprite structure with a lattice constant of a = 4.74 and 4.27 Å, respectively.[1−4] They are the most thermodynamically stable compounds among the corresponding possible oxides, such as Ag_2O_2, Ag_2O_3, and CuO at room temperature, and are used practically as battery electrodes, chemical catalysts, and marine antifoulants. Recently, they have also attracted increasing attention as a promising light-absorption material for photovoltaic devices (PVs) because of their nontoxicity and suitable direct bandgaps of ∼1.3 and ∼2.0 eV for Ag_2O and Cu_2O, respectively. Whereas several techniques such as sputtering deposition,[5,6] chemical vapor deposition (CVD),[7,8] thermal[9,10] or anodic oxidation of a Cu sheet,[11] photochemical deposition,[12] and cathodic electrocrystallization[13,14] have been used to yield polycrystalline Cu_2O films, little has been reported on the direct growth of Ag_2O films except for magnetron sputtering[15] and electron beam evaporation in an oxygen atmosphere.[3] This is mainly due to the difficulty of Ag_2O growth compared with Cu_2O. Ag_2O decomposes at temperatures above 300 °C in the vapor-phase processes,[16] and in solution-based processes, Ag^+ is readily reduced to metallic Ag.[17] Recently, we developed a direct electrocrystallization method of obtaining polycrystalline Ag_2O films from an ammoniacal silver(I) nitrate aqueous solution, making it possible for both semiconducting oxide films, Ag_2O and Cu_2O, to be obtained by the electrochemical technique.[18]

Electrocrystallization from aqueous solution is a powerful technique for growing high-quality semiconducting oxides, and offers epitaxial growth and as a low-cost, low-temperature, and scalable process.[19,20] To date, various binary oxides, such as ZnO,[21,22] CeO_2,[23,24] TiO_2,[25,26] and Ag_2O_2,[27] have been electrochemically prepared using two major strategies: (i) cathodic electrogeneration of base (i.e., the rise of pH on the electrode surface) from dissolved species, such as dissolved oxygen and nitrate ion, and (ii) anodic oxidation of metal ions to give reactive species with a higher oxidation state. The electrocrystallization methods for Ag_2O[18] and Cu_2O[13,14] utilized in this study are, however, different from the strategies mentioned above, and they can be described as (iii) anodic electrogeneration of acid from dissolved species and (iv) cathodic reduction of metal ions to give reactive species with a lower oxidation state, respectively. It should be noted that all these strategies (i−iv) involve a common key reaction, hydroxylation of reactive metal ions and subsequent dehydration:

Received: June 15, 2012
Revised: November 13, 2012
Published: November 29, 2012

$$M^{n+} + nOH^- \rightarrow [M(OH)_n] \rightarrow MO_{n/2} + n/2H_2O \quad (1)$$

Because electrochemical reactions (i.e., redox reactions) are caused on an electrode, crystal growth proceeds only on the electrode surface and, therefore, generally no precipitates generate in the bulk of the solution. In addition, the precise and continuous tune of the reaction rate or redox activity is feasible by adjusting current density or potential applied to the electrode, allowing control of thickness, orientation, and composition of deposits.[19] The crystal growth orientation is particularly important for the quality of a *pn*-junction interface and for the catalytic activity. Since lattice-matched substrates or undercoatings have typically been employed to control the growth orientation, using conventional substrates with a random orientation will extend the application range. According to the well-known geometrical selection growth model for a polycrystalline film formation, if a growth rate is different among crystal planes, the growth proceeds in a direction perpendicular to the plane with the fastest growth rate. This results in an oriented film, even though the initial nuclei have a random orientation.[28] In other words, it is possible that the preferred growth orientation may change depending on the growth condition.

Here we have demonstrated the facile crystal orientation control of Ag_2O and Cu_2O via galvanostatic electrodeposition onto a conventional transparent conductive substrate, F:SnO_2-coated glass (FTO), with a random orientation. The preferred orientation of Ag_2O and Cu_2O is changed between ⟨111⟩ and ⟨100⟩ directions by adjusting the applied current density. A reasonable explanation for the mechanism is also discussed.

2. EXPERIMENTAL SECTION

General Procedures and Electrochemical Measurements. All aqueous solutions were prepared with reagent grade chemicals and deionized water purified by a Milli-RX12 Plus system. F-doped SnO_2-coated glass (FTO; ~10 Ω/□, Nihon Sheet Glass) was used as a working electrode. Before deposition, an FTO substrate was washed ultrasonically in acetone and rinsed with deionized water. The FTO substrate was then electropolished at an anodic current density of 10 mA cm^{-2} in a ~1 M (M = mol dm^{-3}) NaOH solution. Linear-sweep voltammetry (LSV) was carried out in a three-electrode cell using an electrochemical analyzer (HSV-100, Hokuto Denko) with a Pt-sheet counter electrode. The reference electrode used for Ag_2O and Cu_2O deposition was a Pt-wire and a Ag/AgCl electrode, respectively. The electrodeposition of Ag_2O and Cu_2O films was performed galvanostatically in a two-electrode cell using a potentio/galvanostat (HABF5001, Hokuto Denko) with a Pt-sheet counter electrode.

Electrodeposition of Ag_2O. Anodic electrolysis was performed at current densities ranging from 1.0 to 10 mA cm^{-2} at 25 °C using an H-type divided cell separated by a G4 glass-filter, and details of this are provided in previous literature reports.[18] The anode compartment of the H-type cell contained an aqueous 0.2 M $AgNO_3$−0.73 M NH_3 solution with a pH of 12 adjusted with NaOH. *Caution: It is possible that the reaction of high concentration silver nitrate and ammonia or electrolytes left for a long time may give fulminating silver (explosive nature). The electrolytes must be inactivated with chloride salts, such as NaCl, immediately after the experiments.* The cathode compartment contained an aqueous 1.0 M $NaNO_3$ solution. After the electrolysis at a total electric quantity of 5.0 C cm^{-2}, deposits were rinsed with deionized water and then dried under ambient atmosphere.

Electrodeposition of Cu_2O. Cathodic electrolysis was performed at current densities ranging from 0.5 to 4.0 mA cm^{-2} at 60 °C using an undivided cell. The electrolyte used was an aqueous solution containing 0.4 M $CuSO_4 \cdot 5H_2O$ and 3 M lactic acid with a pH of 9 adjusted with KOH. After the electrolysis at a total electric quantity of 2.0 C cm^{-2}, deposits were rinsed with deionized water and then dried under ambient atmosphere.

Characterization of Films. X-ray diffraction (XRD) patterns for the electrodeposited films were measured using a Rigaku RINT 2500 system with monochromated Cu Kα radiation. The surface and cross-sectional images of the films were taken using field emission scanning electron microscopy (FESEM; JSM6700F, JEOL).

3. RESULTS AND DISCUSSION

3.1. Electrodeposition Behavior of Ag_2O and Cu_2O. LSV was performed to determine the applied current density giving Ag_2O and Cu_2O from the corresponding electrolytes. The electrolyte for Ag_2O (pH = 12) consisted of silver(I) nitrate and ammonia, and the electrolyte for Cu_2O (pH = 9) contained cupric sulfate and lactic acid. Complexation of the metal cations with the ligands yielded stable dissolved species, $[Ag(NH_3)_2]^+$ and $Cu(CH_3CHOHCOO)_2$,[18,29,30] in the alkaline solutions. Anodic LSV in the electrolyte for Ag_2O was carried out at 25 °C using a FTO substrate, Pt sheet, and Pt wire as a working, counter, and quasi-reference electrode,[31] respectively. The sweep was started from a rest potential at a scan rate of 5 mV s^{-1} as shown in Figure 1a. Anodic current was observed at

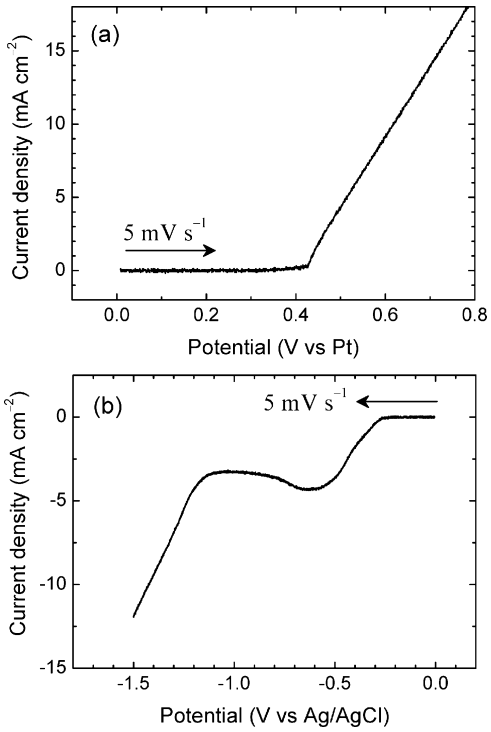

Figure 1. Linear potential sweep voltammograms in (a) an ammoniacal silver(I) nitrate solution for Ag_2O at 25 °C and (b) a cupric sulfate−lactic acid solution for Cu_2O at 60 °C.

0.42 V (vs Pt) or higher and increased linearly without plateau to at least 1.8 V. A dark-gray precipitate was deposited on the FTO substrate simultaneously with the generation of gaseous bubbles, which corresponds to the oxidation reaction of water to give molecular oxygen and protons.[18] Since the bubbles generated intensively and covered the substrate surface at current densities above 10 mA cm^{-2}, the range of applied current density for the Ag_2O electrodeposition was determined to be 1.0−10 mA cm^{-2}. Figure 1b shows cathodic LSV in the electrolyte for Cu_2O at 60 °C using a FTO substrate, Pt sheet, and Ag/AgCl electrode as a working, counter, and reference

dx.doi.org/10.1021/cg300813z | Cryst. Growth Des. 2013, 13, 52−58

electrode, respectively. The sweeping condition was the same as that of Ag_2O. In this case, the steady-state current due to the reduction of cupric complex to Cu^+, which involves Cu_2O deposition, ranged from ~0 to 4.0 mA cm^{-2} and was between −0.3 and −0.6 V (vs Ag/AgCl). A plateau was observed at more negative potentials from −0.6 to −1.1 V probably due to the diffusion-limited condition. The cathodic current then increased abruptly by the deposition of metallic copper. Thus, current densities ranging from 0.5 to 4.0 mA cm^{-2} were applied in the Cu_2O electrodeposition.

Figure 2 shows variation in electrode potential during galvanostatic Ag_2O (anodic electrolysis) and Cu_2O (cathodic

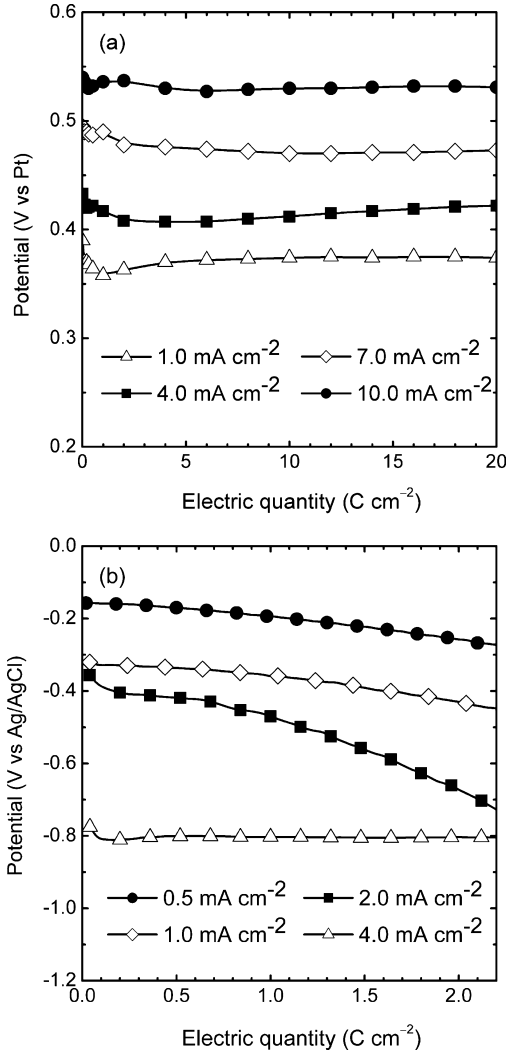

Figure 2. Deposition potential variation during galvanostatic (a) Ag_2O and (b) Cu_2O electrodeposition at four different applied current densities as a function of electric quantity.

electrolysis) electrodeposition at different applied current densities within the range determined above. For Ag_2O (Figure 2a), each potential remained constant up to an electric quantity of 20 C cm^{-2} and increased with increasing applied current density, which is consistent with the LSV results (Figure 1a). This indicates that an oxidation reaction of water occurred continually during the electrolysis. In the case of Cu_2O (Figure 2b), electrode potential for cathodic current densities of 0.5–2.0 mA cm^{-2} shifted gradually to the negative side as electric quantity increased, whereas that for a current density of 4.0 mA cm^{-2} remained constant at −0.8 V. The negative shift is likely due to the diffusion limit of the cupric complex rather than the electrical resistance of the deposits, and the constant potential observed at 4.0 mA cm^{-2} is likely specified by reduction of water, $E(H_2O/H_2)$ = −0.53 V vs Ag/AgCl at pH = 9. The resulting Ag_2O and Cu_2O films showed silicon-like and dark orange-red color, respectively, and had a smooth and homogeneous surface with good adhesion (Figure 3).

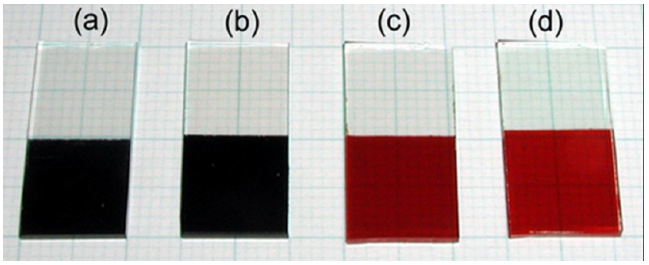

Figure 3. Photographs from the glass side of (a, b) Ag_2O and (c, d) Cu_2O films electrodeposited on FTO substrates at current densities of (a) 1.0, (b) 10, (c) 0.5, and (d) 4.0 mA cm^{-2}.

3.2. Structural Characterization of Ag_2O and Cu_2O Films. Figure 4 shows normalized XRD patterns of the Ag_2O (left) and Cu_2O (right) films electrodeposited galvanostatically on FTO substrates with a passing electric quantity of 5.0 and 2.0 C cm^{-2}, respectively. All diffraction peaks were assigned to either Ag_2O (JCPDS no. 41-1104), Cu_2O (JCPDS no. 05-0667), or FTO, and no other phases, such as metallic silver and copper, were recognized. For the Ag_2O films, the strongest diffraction peak shifted from 111 to 200 with increasing applied current density, whereas it shifted from 200 to 111 for the Cu_2O films. The degree of preferred orientation was estimated

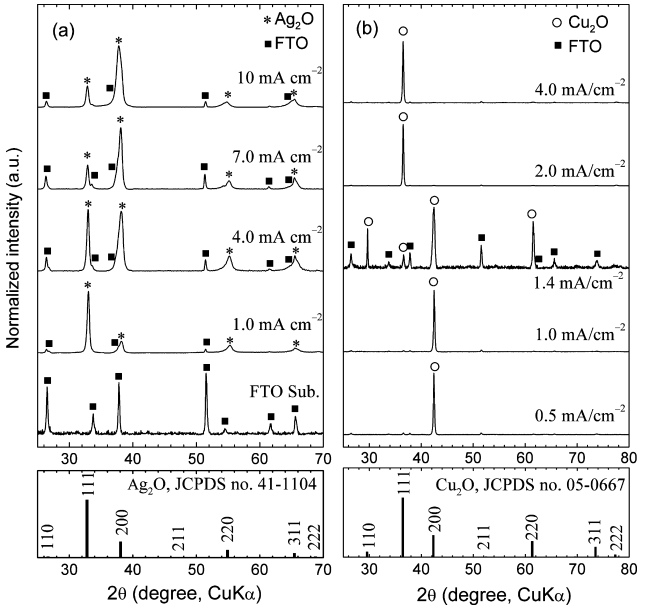

Figure 4. XRD patterns of (a) Ag_2O and (b) Cu_2O films electrodeposited on FTO substrates from an ammoniacal silver(I) nitrate solution at 25 °C and a cupric sulfate–lactic acid solution at 60 °C, respectively, at various applied current densities. The XRD pattern of a FTO substrate and JCPDS data for Ag_2O (no. 41-1104) and Cu_2O (no. 05-0667) are also presented.

dx.doi.org/10.1021/cg300813z | Cryst. Growth Des. 2013, 13, 52–58

quantitatively by calculating Harris texture coefficient, T_c.[32,33] The T_c is defined as

$$T_c(hkl) = n\frac{I_m(hkl)/I_0(hkl)}{\sum_1^n I_m(hkl)/I_0(hkl)} \quad (2)$$

where $I_m(hkl)$ is the measured relative intensity of the peak corresponding to the hkl diffraction, $I_0(hkl)$ is the relative intensity from the same diffraction in the standard powder sample, and n is the total number of diffraction peaks considered in the evaluation. The T_c ranges from 0 to n, and samples having a preferred (hkl) orientation and random orientation exhibit $T_c(hkl)$ values of $\sim n$ and ~ 1, respectively. In the present case, we chose three diffractions (n = 3) of 111, 200, and 220; calculated values for $T_c(111)$ and $T_c(100)$ are plotted in Figure 5, indicating shallow and sharp changes

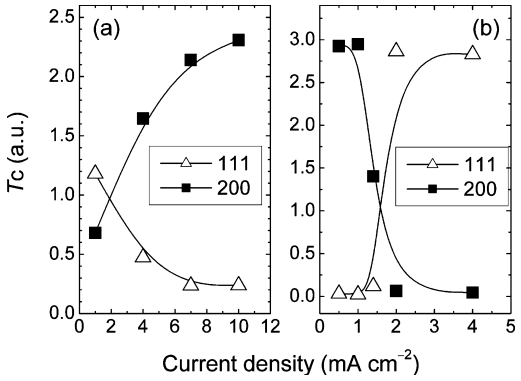

Figure 5. Variation of texture coefficient, T_c, for 111 and 200 diffractions of (a) Ag_2O and (b) Cu_2O films. These values are calculated from the XRD patterns in Figure 4.

depending on the current density for the Ag_2O and Cu_2O films, respectively. Whereas Cu_2O showed almost maximum T_c values ($\sim$3) for each orientation, smaller T_c values, especially for the ⟨111⟩ orientation, were obtained in Ag_2O. Figure 5a implies that the deposition of highly ⟨111⟩-oriented Ag_2O is expected at much lower current densities, i.e., below 1 mA cm^{-2}. However, lower current densities were not able to deposit continuous Ag_2O films due to the insufficient driving force required for the deposition. Furthermore, the shallow behavior for Ag_2O is attributed to its deposition mechanism, where the applied anodic current indirectly affects the deposition, as is discussed later. Each T_c value pointed by the intersection of two curves is almost 1, suggesting that randomly oriented films will be obtained at a current density of 1.7−2.0 mA cm^{-2} for both oxides. Thus, the XRD study clearly shows that the preferred growth orientation can be readily controlled by only adjusting the applied current density.

Top-view FESEM images of the Ag_2O and Cu_2O films are shown in Figure 6. All the surfaces of these polycrystalline films are well-faceted and continuous over the entire substrate. The surface morphology of Ag_2O, to a varying degree, contained both four-sided pyramidal grains and plane-triangular grains. In contrast, Cu_2O showed clear morphological differences depending on the current density: four-sided pyramid (0.5 mA cm^{-2}), plane square (1 mA cm^{-2}), plane triangle (2 mA cm^{-2}), and a three-sided pyramid (4 mA cm^{-2}). The observed plane square corresponds to the (100) planes, and the side faces of the four-sided pyramid are relevant to the (111) plane,[14] indicating that the grains grow in the ⟨100⟩ direction.

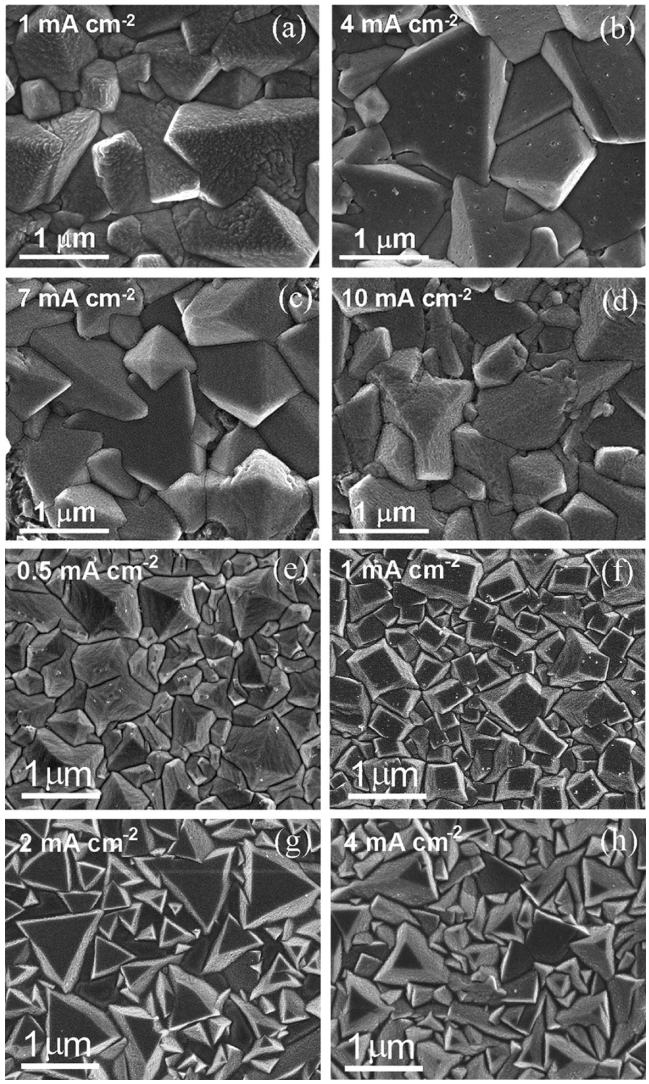

Figure 6. Top-view FESEM images of (a−d) Ag_2O and (e−h) Cu_2O films electrodeposited on FTO substrates from an ammoniacal silver(I) nitrate solution at 25 °C and a cupric sulfate−lactic acid solution at 60 °C, respectively, at various current densities.

On the other hand, the plane triangle corresponds to the (111) plane, and the side faces of the three-sided pyramid are relevant to the (100) plane, indicating that the grains grow in the ⟨111⟩ direction. Such a drastic change in the crystal shape typically seen in Cu_2O is attributed to a growth-rate ratio between ⟨100⟩ and ⟨111⟩ directions, $v_{\langle 100\rangle}/v_{\langle 111\rangle}$, as reported by Switzer and co-workers,[34] who employed a computer simulation that indicated the crystal shapes change from cubic to octahedral with increasing the $v_{\langle 100\rangle}/v_{\langle 111\rangle}$ value.

Figure 7 shows the corresponding cross-sectional FESEM images. In all of the films, there are no distinct grain boundaries crossing in a direction parallel to the substrate surface, suggesting that the preferred orientation is developed at an early stage and is maintained during the growth. The thickness of the Ag_2O films deposited by passing an electric quantity of 5 C cm^{-2} was approximately 1 μm irrespective of the applied current density ranging from 1.0 to 10 mA cm^{-2}. The Cu_2O films deposited by passing an electric quantity of 2 C cm^{-2} at current densities of 0.5−2.0 mA cm^{-2} also had approximately the same thickness ($\sim$2.5 μm, cross-sectional Cu_2O FESEM images for 1.0−2.0 mA cm^{-2} are not shown here; see

dx.doi.org/10.1021/cg300813z | Cryst. Growth Des. 2013, 13, 52−58

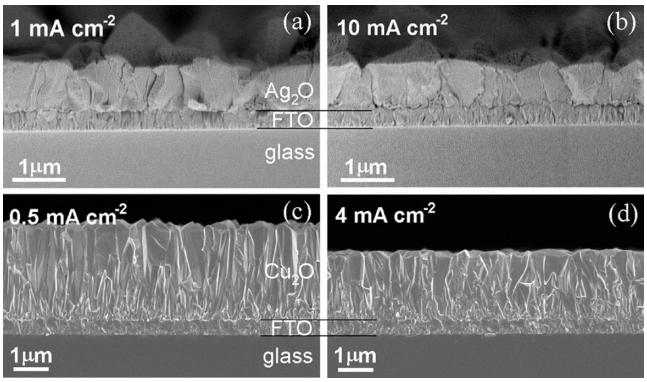

Figure 7. Cross-sectional FESEM images of (a, b) Ag_2O and (c, d) Cu_2O films electrodeposited on FTO substrates from an ammoniacal silver(I) nitrate solution at 25 °C and a cupric sulfate–lactic acid solution at 60 °C, respectively, at various current densities.

Supporting Information). These results indicate that the amount of the deposits depends on the total passing electric quantity and has no relation to the applied current density. Nevertheless the thickness of Cu_2O was exceptionally reduced to 2.0 μm at a current density of 4.0 mA cm^{-2} (Figure 7d). The decrease in thickness at the higher current density is due to the side reaction of water reduction, as mentioned above. Since the deposition mechanisms of Ag_2O and Cu_2O are quite different each other, as is discussed later, their growth rates should also be different, even at equal current density. Indeed, the apparent current efficiency of the Ag_2O and Cu_2O deposition is estimated to be approximately 24 and 100%, respectively. This calculation is based on Faraday's laws of electrolysis, and the assumption that the Ag_2O and Cu_2O depositions are four- and two-electron reactions, respectively.

3.3. Electrodeposition Mechanism and Preferred Orientation Change. According to the thermodynamic equilibrium model for crystal growth, a difference in crystal growth rate among crystal planes depends on their surface energy; crystallization rate in a direction perpendicular to a crystal plane with a higher surface energy is faster, which minimizes its surface area and the total surface energy. As a consequence of the two crystal-growth models, i.e., geometrical selection and thermodynamic equilibrium, films grow spontaneously with a preferred orientation perpendicular to a higher surface energy plane under an appropriate condition. For instance, in the case of ZnO with a hexagonal wurtzite structure, the polar (0001) plane has a higher surface energy than the nonpolar $(10\bar{1}0)$ plane, leading to hexagonal columnar ZnO grains grown along the ⟨0001⟩ direction.[35] However, the preferred orientation as well as the degree of ⟨0001⟩ orientation can be changed depending on the electrodeposition conditions, including current density and growth temperature.[36] In the case of Ag_2O and Cu_2O with a cubic cuprite structure, the polar (100) plane has a higher surface energy than that of the nonpolar (111) plane.[37−39] Thus, in a simple thermodynamic equilibrium state, ⟨100⟩-oriented films could be expected, and ⟨111⟩-oriented films could be responsible for a nonequilibrium state, i.e., under a kinetic control.

The cathodic electrodeposition of Cu_2O from an alkaline cupric sulfate–lactic acid solution can be described as

$$Cu^{2+} + 2L^- \rightarrow [Cu^{II} - L_2] \qquad (L^-: \text{lactate ion}) \tag{3}$$

$$[Cu^{II} - L_2] + e^- \rightarrow Cu^+ + 2L^- \qquad ([Cu^{II} - L_2]: \text{cupric lactate complex}) \tag{4}$$

$$Cu^+ + OH^- \rightarrow [Cu^{I}OH] \tag{5}$$

$$2[Cu^{I}OH] \rightarrow Cu_2O + H_2O \tag{6}$$

Complexation of Cu^{2+} with lactate ion yields cupric lactate complex and allows an alkaline aqueous solution containing dissolving Cu^{2+} species without precipitation. The cupric lactate complex is reduced on an electrode to give reactive Cu^+, which is hydroxylated to deposit CuOH, and then Cu_2O is formed by dehydration. Thus, the applied current directly affects the generation of the reactive metal cation. The elementary formation rate of $Cu^{I}OH$, a precursor of Cu_2O, on a FTO substrate can be expressed as

$$v_{(CuOH)} = k[Cu^+][OH^-] \tag{7}$$

where k is a rate constant. Since the concentration of hydroxide ions, $[OH^-]$, was constant in the present experiment (pH = 9), eq 7 can be transformed to $v_{(CuOH)} = k'[Cu^+]$. The ∼100% current efficiency in the Cu_2O electrodeposition implies that the electron supplied to FTO should be exclusively consumed to reduce the cupric lactate complex to Cu^+ (eq 4), and the subsequent deposition reactions (reaction 5) proceed quantitatively. Thus, the generation rate of Cu^+ in the vicinity of FTO is proportional to applied current density, J, and $v_{(CuOH)}$ increases with $[Cu^+]$, giving a proportional relation between $v_{(CuOH)}$ and J, $v_{(CuOH)} \propto J$. In the experimental results obtained here, when $v_{(CuOH)}$ is lower (i.e., at lower J), ⟨100⟩ preferred orientation was obtained, while ⟨111⟩ growth orientation was preferred at higher $v_{(CuOH)}$ (i.e., at higher J) (see Figure 5b). A similar trend has also been observed in a different substrate of stainless steel.[34] Furthermore, when the electrodeposition was performed at a higher pH of 12, where $v_{(CuOH)}$ becomes 10^3 times higher than that at pH = 9, only Cu_2O with a ⟨111⟩ preferred orientation was obtained, even at lower J (0.5 mA cm^{-2}) and also at 4.0 mA cm^{-2} (XRD patterns of Cu_2O films electrodeposited at pH = 12 are shown in Supporting Information). Thus, the trend of the preferred growth orientation between ⟨100⟩ and ⟨111⟩ directions can be explained qualitatively by considering the elementary formation rate of CuOH ($v_{(CuOH)} = k[Cu^+][OH^-]$) and is consistent with the crystal growth model mentioned above; lower $v_{(CuOH)}$ corresponds to a thermodynamic equilibrium control, giving ⟨100⟩ orientation, while higher $v_{(CuOH)}$ is under a kinetic control, giving ⟨111⟩ orientation.

On the other hand, a possible mechanism for the anodic electrodeposition of Ag_2O from an ammoniacal silver(I) nitrate solution (pH = 12) has been proposed in our previous study:[18]

$$Ag^+ + 2NH_3 \rightarrow [Ag^{I}(NH_3)_2]^+ \tag{8}$$

$$H_2O \rightarrow 2H^+ + 1/2O_2 + 2e^- \tag{9}$$

$$[Ag^{I}(NH_3)_2]^+ + 2H^+ \leftrightarrow Ag^+ + 2NH_4^+ \tag{10}$$

$$H^+ + OH^- \leftrightarrow H_2O \tag{11}$$

$$NH_3 + H_2O \leftrightarrow NH_4^+ + OH^- \tag{12}$$

$$Ag^+ + OH^- \rightarrow [Ag^{I}OH] \tag{13}$$

dx.doi.org/10.1021/cg300813z | Cryst. Growth Des. 2013, 13, 52−58

$$2[Ag^{I}OH] \rightarrow Ag_2O + H_2O \quad (14)$$

In this case, anodic current oxidizes water not the ammonia silver complex, $[Ag^{I}(NH_3)_2]^+$, to yield protons in the vicinity of a FTO substrate. Taking into account the fact that the current efficiency is as low as 24%, the mechanism should involve side and reverse reactions. Thus, a portion of the protons react with the silver(I) complex to give transient free Ag^+ (eq 10), and the rest will react with hydroxide ions (eq 11), where the local consumption of OH^- can be compensated by excess NH_3 (eq 12) and/or the diffusion of OH^- from the bulk solution (pH = 12). A portion of the free Ag^+ ions are then hydroxylated to form AgOH (eq 13), and the rest will reform the complex. From eq 13, the elementary formation rate of AgOH can be expressed as $v_{(AgOH)} = k[Ag^+][OH^-]$, which is the same as that of Cu_2O. However, with AgOH, the relationship between applied current density J and $v_{(AgOH)}$ is not as simple when compared with that for Cu_2O. On the basis of the proposed mechanism (eqs 9−11), an increase in anodic current decreases local $[OH^-]$, while reactive $[Ag^+]$ is increased; i.e., the $[OH^-]$ and $[Ag^+]$ near the electrode vary in opposite directions depending on J. Since the resulting film thickness, after passing the constant electric charge, is nearly the same irrespective of J, the total amount of Ag^+ that reacted with OH^- should also be approximately the same irrespective of J, indicating that the generation rate of Ag^+ (eq 10) and the consumption rate of OH^- by the generated protons (eq 11) will be linearly proportional to J. Whereas local $[Ag^+]$ is thus linearly increased with increasing J, the decrease of local $[OH^-]$ is nonlinear due to the compensation effect of NH_3 (eq 12) as well as the diffusion of OH^- from the bulk solution. These recovery effects on the local pH are likely more pronounced when the consumption rate of OH^- is lower, i.e., at lower J, because there is more time to recovery. Thus, the elementary formation rate of $v_{(AgOH)}$ will increase nonlinearly with decreasing J. In the Ag_2O electrodeposition here, lower and higher J, i.e., higher and lower $v_{(AgOH)}$, yielded ⟨111⟩ and ⟨100⟩ preferred growth orientations, respectively, and the trend between $v_{(AgOH)}$ and growth orientation is consistent with that for Cu_2O.

4. CONCLUSIONS

In this paper, we have demonstrated that the preferred orientation of Ag_2O and Cu_2O polycrystalline films electrodeposited galvanostatically on FTO substrates was changed between ⟨111⟩ and ⟨100⟩ by simply adjusting the applied current density. The range of the applied current density for the Ag_2O and Cu_2O electrodeposition was determined by LSV in electrolytes of an ammoniacal silver(I) nitrate solution (pH = 12) and a cupric sulfate−lactic acid solution (pH = 9) to be 1.0−10 mA cm^{-2} and 0.5−4.0 mA cm^{-2}, respectively. The XRD patterns of the obtained films showed that the strongest diffraction peak was changed from ⟨111⟩ to ⟨100⟩ with increasing and decreasing current density for Ag_2O and Cu_2O, respectively. The degree of preferred orientation was estimated by calculating the texture coefficient, T_c, and this revealed a clear change in preferred orientation between ⟨111⟩ and ⟨100⟩ with applied current density. Surface crystal morphology, especially for the Cu_2O films, was also changed from a four-sided pyramidal shape to a three-sided pyramidal shape, corresponding to the change in preferred orientation. Deposition current efficiency was estimated based on Faraday's laws to be approximately 24 and 100% for the Ag_2O and Cu_2O, respectively. On the basis of each electrodeposition mechanism and well-known crystal growth models, we found that the observed trend of the preferred orientation can be reasonably explained by considering the formation rate of hydroxides, $v_{(MOH)} = [Mn^+][OH^-]$; higher and lower $v_{(MOH)}$ yield ⟨111⟩ and ⟨100⟩ preferred orientations, respectively, which is applicable to both Ag_2O and Cu_2O. The results obtained here will be useful in understanding the evolution of preferred growth orientation on randomly oriented substrates by electrocrystallization and also to improve device performances.

■ ASSOCIATED CONTENT

Supporting Information

The cross-sectional FESEM images of Cu_2O films electrodeposited at 1.0−2.0 mA cm^{-2} and the XRD patterns of Cu_2O films electrodeposited from an electrolyte at pH = 12. This material is available free of charge via the Internet at http://pubs.acs.org.

■ AUTHOR INFORMATION

Corresponding Author

*E-mail: tshina@omtri.or.jp.

Notes

The authors declare no competing financial interest.

■ ACKNOWLEDGMENTS

This work was supported in part by the NEDO under the METI Japan.

■ REFERENCES

(1) Fortiu, E.; Weichman, F. L. *Phys. Status Solidi A* **1964**, *5*, 515.
(2) Tjeng, L.; Meinders, M.; Van Elp, J.; Ghijsen, J.; Sawatzky, G.; Johnson, R. *Phys. Rev. B* **1990**, *41*, 3190.
(3) Bock, F.; Christensen, T.; Rivers, S.; Doucette, L.; Lad, R. *Thin Solid Films* **2004**, *468*, 57.
(4) Rakhshani, A. *Solid-State Electronics* **1986**, *29*, 7.
(5) Drobny, V.; Pulfrey, L. *Thin Solid Films* **1979**, *61*, 89.
(6) Pierson, J.; Thobor-Keck, A.; Billard, A. *Appl. Surf. Sci.* **2003**, *210*, 359.
(7) Condorelli, G. G.; Malandrino, G.; Fragala, I. *Chem. Mater.* **1995**, *7*, 2096.
(8) Ottosson, M.; Carlsson, J. O. *Surf. Coat. Technol.* **1996**, *78*, 263.
(9) Li, J.; Vizkelethy, G.; Revesz, P.; Mayer, J.; Tu, K. *J. Appl. Phys.* **1991**, *69*, 1020.
(10) Roos, A.; Chibuye, T.; Karlsson, B. *Solar Energy Mater.* **1983**, *7*, 453.
(11) Fortin, E.; Masson, D. *Solid-State Electronics* **1982**, *25*, 281.
(12) Izaki, M.; Mizuno, K.; Shinagawa, T.; Inaba, M.; Tasaka, A. *J. Electrochem. Soc.* **2006**, *153*, C668.
(13) Rakhshani, A.; Varghese, J. *Solar Energy Mater.* **1987**, *15*, 237.
(14) Golden, T. D.; Shumsky, M. G.; Zhou, Y.; VanderWerf, R. A.; Van Leeuwen, R. A.; Switzer, J. A. *Chem. Mater.* **1996**, *8*, 2499.
(15) Pierson, J.; Rousselot, C. *Surf. Coat. Technol.* **2005**, *200*, 276.
(16) Weaver, J. F.; Hoflund, G. B. *J. Phys. Chem.* **1994**, *98*, 8519.
(17) Pourbaix, M. *Atlas of Electrochemical Equilibria in Aqueous Solutions*; NACE: Houston, TX, 1974.
(18) Ida, Y.; Watase, S.; Shinagawa, T.; Watanabe, M.; Chigane, M.; Inaba, M.; Tasaka, A.; Izaki, M. *Chem. Mater.* **2008**, *20*, 1254.
(19) Therese, G. H. A.; Kamath, P. V. *Chem. Mater.* **2000**, *12*, 1195.
(20) Lincot, D. *Thin Solid Films* **2005**, *487*, 40.
(21) Izaki, M.; Omi, T. *Appl. Phys. Lett.* **1996**, *68*, 2439.
(22) Peulon, S.; Lincot, D. *Adv. Mater.* **1996**, *8*, 166.
(23) Switzer, J. A. *Am. Ceram. Soc. Bull.* **1987**, *66*, 1521.
(24) Li, F. B.; Newman, R.; Thompson, G. *Electrochim. Acta* **1997**, *42*, 2455.
(25) Zhitomirsky, I.; Gal-Or, L.; Kohn, A.; Hennicke, H. *J. Mater. Sci.* **1995**, *30*, 5307.

(26) Natarajan, C.; Nogami, G. *J. Electrochem. Soc.* **1996**, *143*, 1547.
(27) Breyfogle, B. E.; Hung, C. J.; Shumsky, M. G.; Switzer, J. A. *J. Electrochem. Soc.* **1996**, *143*, 2741.
(28) Grigoriev, D. P. *Ontogeny of Minerals*; Israel Program for Scientific Translations: Jerusalem, 1965.
(29) Singh, K.; Jain, S.; Sakore, T.; Biswas, A. *Z. Kristallogr.* **1975**, *141*, 473.
(30) Leopold, S.; Herranen, M.; Carlsson, J. O.; Nyholm, L. *J. Electroanal. Chem.* **2003**, *547*, 45.
(31) Bard, A.; Faulkner, L. *Electrochemical Methods: Fundamentals and Applications*, 2nd ed.; John Wiley & Sons: New York, 2001; pp 53−54.
(32) Jones, M.; McColl, I.; Grant, D. *Surf. Coat. Technol.* **2000**, *132*, 143.
(33) Korotkov, R.; Ricou, P.; Farran, A. *Thin Solid Films* **2006**, *502*, 79.
(34) Zhou, Y.; Switzer, J. A. *Mater. Res. Innovations* **1998**, *2*, 22.
(35) Shinagawa, T.; Watase, S.; Izaki, M. *Cryst. Growth Des.* **2011**, *11*, 5533.
(36) Shinagawa, T.; Chigane, M.; Murase, K.; Izaki, M. *J. Phys. Chem. C* **2012**, *116*, 15925.
(37) Jones, P. M.; Jennifer, A.; Reitz, J. B.; Solomon, E. I. *J. Am. Chem. Soc.* **1998**, *120*, 1506.
(38) Scarano, D.; Bordiga, S.; Lamberti, C.; Spoto, G.; Ricchiardi, G.; Zecchina, A.; Otero Arean, C. *Surf. Sci.* **1998**, *411*, 272.
(39) Soon, A.; Todorova, M.; Delley, B.; Stampfl, C. *Phys. Rev. B* **2007**, *75*, 125420.